Elimination of Nonphysical Solutions and Implementation of Adaptive Step Size Algorithm in Time-Stepping Finite-Element Method for Magnetic Field–Circuit–Motion Coupled Problems

W. N. Fu and S. L. Ho

Electrical Engineering Department, The Hong Kong Polytechnic University, Hung Hom, Kowloon, Hong Kong

The time-stepping finite-element method (FEM) has become a powerful tool in solving transient electromagnetic fields. The formulation can include complex issues such as time harmonics and space harmonics, nonlinear magnetic property of iron materials, external circuit, and mechanical motion in the system equations. However, as the derivatives of physical quantities are usually unknown at the initial step of the time-stepping method, erroneous solutions might appear at the beginning of the transient process. To reduce the number of time steps, an adaptive step size algorithm can be used. In this paper, a method to eliminate the nonphysical or nonrealistic solutions at the start of the time-stepping finite-element analysis (FEA), when simulating the transient process of electric devices, is presented. A practical implementation of adaptive time step size algorithm for coupled problems is proposed. A matrix operation method, which can be understood clearly and implemented easily, that deals with matching boundary conditions in the study of mechanical motion, is also described.

***Index Terms*—Adaptive algorithm, coupling method, electric circuit, electric device, finite-element method, initialization, magnetic field, mechanical motion, time-stepping.**

I. Introduction

THE TIME-STEPPING finite-element method (FEM), which couples magnetic field with electric circuit and mechanical force/torque balance equations, has been widely used to simulate transient operation of electric devices [1]–[7]. As with all numerical methods, it is crucial to increase the accuracy of the solution with minimal computing effort and FEM is no exception. A formulation for magnetic field—arbitrary connected electric circuit coupled problems, which has symmetrical coefficient matrix in the system equations, has been presented [8]. The formulation is further enhanced to improve its nonlinear convergence while reducing the numerical error of its derivative quantities [9]. An adaptive time step size algorithm is also proposed to reduce the computing time [10].

At the starting point of time stepping (time $t = 0$), the solution may well be incorrect because the time derivatives of some physical quantities are unknown. For adaptive time-stepping method, because of the presence of complicated physical quantities in the field–circuit–motion coupled models, there are indeed many practical problems that must be addressed thoroughly and carefully in the implementation of the adaptive time-stepping methodology.

A method to initialize the time-stepping FEM solver for magnetic field–electric circuit–mechanical motion coupled problems is proposed in this paper to eliminate the nonphysical solutions. A practical, effective and robust implementation method of the adaptive time stepping algorithm is also described. The merits of the proposed method are: 1) the criterion of the step size control is suitable for coupled system equations having different physical quantities, such as magnetic vector potential, electric current and rotor position; 2) smart control of the step size ensures that the accuracy of the indirect coupling with the mechanical balance equation is high; 3) the discretization error of the excitations is also included in the choice of the step size; and 4) some special measures are added to prevent unrealistic sharp changes that might give rise to unduly small step size. A matrix operation method is also described to simply and clearly deal with matching boundary conditions in the study of mechanical motion.

Manuscript received June 23, 2009; revised August 08, 2009. Current version published December 23, 2009. Corresponding author: W. N. Fu (e-mail: eewnfu@polyu.edu.hk).

Color versions of one or more of the figures in this paper are available online at http://ieeexplore.ieee.org.

Digital Object Identifier 10.1109/TMAG.2009.2030678

II. Basic System Equations

A. System Equations

The proposed method can be applied to both two-dimensional (2-D) and three-dimensional (3-D) FEM. For simplicity, the discussion will be limited to a 2-D problem defined in the x-y plane. For completeness of this paper, the basic equations of transient magnetic field–electric circuit coupled problem are summarized as magnetic field equation [11]–[16]

$$lp\nabla\cdot(\nu\nabla A) - lp\sigma\frac{\partial A}{\partial t} + \frac{ld_pN}{Sa}i_{\rm ad} + \frac{ld_pN}{Sa}i_w = -lp\nu\mu_0\left(\frac{\partial M_y}{\partial x} - \frac{\partial M_x}{\partial y}\right) \quad (1)$$

together with an additional equation

$$-\frac{ld_pN}{Sa}\iint_\Omega \frac{\partial A}{\partial t}{\rm d}\Omega + R_{\rm dc}i_{ad} = 0 \quad (2)$$

and an electric circuit branch equation

$$-\frac{ld_pN}{Sa}\iint_\Omega \frac{\partial A}{\partial t}{\rm d}\Omega - R_{\rm dc}i_w = -u_w \quad (3)$$

where l is the depth of the model in the z-direction; p is the symmetry multiplier which is defined as the ratio of the original full cross-sectional area to the solution area; ν is the reluctivity of material and σ is its conductivity; A is the z-component of the

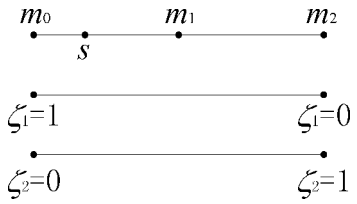

Fig. 1. The matching boundary condition.

magnetic vector potential; d_p is the polarity ($+1$ or -1) to represent, respectively, the forward paths or return paths of the windings; S is the total cross-sectional area of the region occupied by the winding in the solution domain; N is the total conductor number of this winding; a is the number of parallel branches in the winding; $R_{\rm dc}$ is the dc resistance of the winding; i_w and u_w are the branch current and voltage of the winding, respectively; μ_0 is the magnetic permeability in vacuum; M_x and M_y are, respectively, the x- and y-components of the magnetization vector (amperes/meter) in the permanent magnets (PM). If the external circuit equations are established by using the loop method, the additional (2) and the additional current $i_{\rm ad}$ are introduced in regions of solid conductors to ensure the last coefficient matrix of the field-circuit coupled equations is symmetrical [8]. Moreover, the rationale for multiplying the depth of the model l to all terms in (1) is to generalize the formulation [14]. If there are minor differences in the model depths among different objects, the formulation still works for 2-D models. With the terms formulated in (1), the integration will be on volume, instead of on surfaces as in normal 2-D methods. The second rationale of the multiplication operation is to make the last coefficient matrix of the field-circuit coupled system equation symmetrical. The dimensions of (2) and (3) are voltages. If the depth of the model l is multiplied to each and every term in (1), the coupling terms of the magnetic field and the electric circuit in the last system equations will be the same [14].

Using the Galerkin method to discretize the field equation, the coupled field and circuit equations in the magnetic field regions can be written in matrix format as [8]

$$\begin{bmatrix} \boldsymbol{C}_{11} & -\boldsymbol{C}_{12} & -\boldsymbol{C}_{13} \\ 0 & -\boldsymbol{C}_{22} & 0 \\ 0 & 0 & -\boldsymbol{C}_{33} \end{bmatrix} \begin{Bmatrix} \boldsymbol{A} \\ \boldsymbol{i}_{\rm ad} \\ \boldsymbol{i}_w \end{Bmatrix} + \begin{bmatrix} \boldsymbol{D}_{11} & 0 & 0 \\ -\boldsymbol{D}_{21} & 0 & 0 \\ -\boldsymbol{D}_{31} & 0 & 0 \end{bmatrix} \begin{Bmatrix} \frac{\mathrm{d}\boldsymbol{A}}{\mathrm{d}t} \\ \frac{\mathrm{d}\boldsymbol{i}_{\rm ad}}{\mathrm{d}t} \\ \frac{\mathrm{d}\boldsymbol{i}_w}{\mathrm{d}t} \end{Bmatrix} = \begin{Bmatrix} \boldsymbol{P}_1 \\ 0 \\ -\boldsymbol{u}_w \end{Bmatrix} \quad (4)$$

where the coefficient sub-matrixes $\boldsymbol{C}_{11} = \boldsymbol{C}_{11}^T, \boldsymbol{C}_{22} = \boldsymbol{C}_{22}^T, \boldsymbol{C}_{33} = \boldsymbol{C}_{33}^T, \boldsymbol{D}_{11} = \boldsymbol{D}_{11}^T, \boldsymbol{C}_{12} = \boldsymbol{D}_{21}^T$ and $\boldsymbol{C}_{13} = \boldsymbol{D}_{31}^T$; $\boldsymbol{P}_1$ is associated with the excitations of PM.

Adding the external circuit equations into (4) and using the loop method, one has [9]

$$\begin{bmatrix} \boldsymbol{C}_{11} & -\boldsymbol{C}_{12} & -\boldsymbol{C}_{1l} \\ 0 & -\boldsymbol{C}_{22} & 0 \\ 0 & 0 & -\boldsymbol{C}_{ll} \end{bmatrix} \begin{Bmatrix} \boldsymbol{A} \\ \boldsymbol{i}_{\rm ad} \\ \boldsymbol{i}_l \end{Bmatrix} + \begin{bmatrix} \boldsymbol{D}_{11} & 0 & 0 \\ -\boldsymbol{D}_{21} & 0 & 0 \\ -\boldsymbol{D}_{l1} & 0 & 0 \end{bmatrix} \begin{Bmatrix} \frac{\mathrm{d}\boldsymbol{A}}{\mathrm{d}t} \\ \frac{\mathrm{d}\boldsymbol{i}_{\rm ad}}{\mathrm{d}t} \\ \frac{\mathrm{d}\boldsymbol{i}_l}{\mathrm{d}t} \end{Bmatrix} = \begin{Bmatrix} \boldsymbol{P}_1 \\ 0 \\ -\boldsymbol{P}_l \end{Bmatrix} \quad (5)$$

where $\boldsymbol{i}_l$ is the loop current; $\boldsymbol{P}_l$ is associated with the excitations in the external circuit.

Because the time constant of the mechanical system is much larger than those of the magnetic field and electric circuit system, the mechanical force balance equation for translational motion and the mechanical torque balance equation for rotation are coupled to the system equations indirectly [17] in order to keep the positions of the moving objects constant during the nonlinear iteration at each time step.

B. Matching Boundary Conditions

At the interface between the moving objects and the background, the solutions are connected by a matching boundary condition. The nodes on the background side of the interface are called master nodes; the nodes on the moving objects' side of the interface are called slave nodes. The variables on the slave nodes are depending on the variables of the master nodes and hence are not solved. All contributions from the element assembly to the slave nodes will be added to the associated master nodes. In Fig. 1, the master nodes on the edge of a triangle are m_0, m_1, m_2 (m_1 is the middle point of the edge); the slave node on the edge of the neighbor triangle is s.

The variable A_s on the slave node can be expressed as

$$A_s = N_{m0}A_{m0} + N_{m1}A_{m1} + N_{m2}A_{m2} \quad (6)$$

where the shape functions are

$$N_{m0} = \zeta_1(2\zeta_1 - 1), \quad (7)$$
$$N_{m1} = 4\zeta_1\zeta_2, \quad (8)$$
$$N_{m2} = \zeta_2(2\zeta_2 - 1). \quad (9)$$

The local coordinates are

$$\zeta_2 = \frac{\sqrt{(x_s - x_{m0})^2 + (y_s - y_{m0})^2}}{\sqrt{(x_{m2} - x_{m0})^2 + (y_{m2} - y_{m0})^2}}, \quad (10)$$
$$\zeta_1 = 1 - \zeta_2 \quad (11)$$

where $(x_s, y_s), (x_{m0}, y_{m0})$ and (x_{m2}, y_{m2}) are the coordinates on the nodes s, m_0 and m_2, respectively. In the system equations, A_s will be replaced by A_{m0}, A_{m1} and A_{m2}. Here a first-order element is taken as an example. The element on the moving object has three nodes: 0, 1, and 2. The slave node 2 is on the motion side of the interface. The system equation can be expressed as (only the entries associated with this element are listed):

$$\begin{bmatrix} \vdots & & \vdots \\ \cdots & \begin{pmatrix} S_{00} & S_{01} & S_{02} \\ S_{10} & S_{11} & S_{12} \\ S_{20} & S_{21} & S_{22} \end{pmatrix} & \cdots \\ \vdots & & \vdots \end{bmatrix} \begin{bmatrix} \vdots \\ \begin{pmatrix} A_0 \\ A_1 \\ A_2 \end{pmatrix} \\ \vdots \end{bmatrix} = \begin{bmatrix} \vdots \\ \begin{pmatrix} P_0 \\ P_1 \\ P_2 \end{pmatrix} \\ \vdots \end{bmatrix}. \quad (12)$$

The edge of the neighbor element has the nodes m_0, m_1, m_2, which are master nodes. A_2 will be replaced by A_{m0}, A_{m1} and

A_{m2}. The transformation relationship is

$$\begin{bmatrix} A_0 \\ A_1 \\ A_2 \end{bmatrix} = \begin{bmatrix} 1 & 0 & 0 & 0 & 0 \\ 0 & 1 & 0 & 0 & 0 \\ 0 & 0 & N_{m0} & N_{m1} & N_{m2} \end{bmatrix} \begin{bmatrix} A_0 \\ A_1 \\ A_{m0} \\ A_{m1} \\ A_{m2} \end{bmatrix} = M \begin{bmatrix} A_0 \\ A_1 \\ A_{m0} \\ A_{m1} \\ A_{m2} \end{bmatrix} \tag{13}$$

where the transformation matrix is defined as

$$M = \begin{bmatrix} 1 & 0 & 0 & 0 & 0 \\ 0 & 1 & 0 & 0 & 0 \\ 0 & 0 & N_{m0} & N_{m1} & N_{m2} \end{bmatrix}. \tag{14}$$

Substituting the above relationship into (13), and multiplying M^T to both sides of the sub-matrix from the row of A_0 to the row of A_{m2}, one has

$$\begin{bmatrix} \vdots & & \vdots \\ \cdots & M^T \begin{pmatrix} S_{00} & S_{01} & S_{02} \\ S_{10} & S_{11} & S_{12} \\ S_{20} & S_{21} & S_{22} \end{pmatrix} M & \cdots \\ \vdots & & \vdots \end{bmatrix} \begin{bmatrix} \vdots \\ \begin{pmatrix} A_0 \\ A_1 \\ A_{m0} \\ A_{m1} \\ A_{m2} \end{pmatrix} \\ \vdots \end{bmatrix} = \begin{bmatrix} \vdots \\ M^T \begin{pmatrix} P_0 \\ P_1 \\ P_2 \end{pmatrix} \\ \vdots \end{bmatrix}. \tag{15}$$

Substituting (14) into the above matrix equation, one has (16), shown at the bottom of the page.

The matrix equation (17) can be further expressed as (18), shown at the bottom of the page.

The coefficient matrix of the system equations is still symmetrical.

III. Initialization of the FEM Solver

A. No Mechanical Motion

At the first step of time-stepping FEM ($t = 0$), the derivatives of the physical quantities with respect to time, such as $\partial \boldsymbol{A}/\partial t$, and $\partial i/\partial t$ (where $\boldsymbol{A}$ is the magnetic vector potential and i is the electric current) are unknown. At the starting point of simulation, the magnetic field is assumed to be at steady state. $\partial \boldsymbol{A}/\partial t$ is thus zero and there is no eddy current in the conductors. There is no induced back electromotive force (EMF) in the windings. All circuit couplings are disabled. Only the magnetostatic field needs to be solved. The magnetic filed is excited by the initial currents in windings and the magnetization of PM materials. That means all windings that have current sources will have initial values of $i = i(0)$.

At the first step, the setup of the model is automatically modified inside the solver as summarized below:

1) The conductivities of all materials are set to zero, thereby making $\partial \boldsymbol{A}/\partial t$ equal to zero.
2) All circuit equations are removed.
3) In the winding regions, the current excitations are assumed to have their initial current values.

$$\begin{bmatrix} \vdots & & \vdots \\ \cdots & \begin{pmatrix} 1 & 0 & 0 \\ 0 & 1 & 0 \\ 0 & 0 & N_{m0} \\ 0 & 0 & N_{m1} \\ 0 & 0 & N_{m2} \end{pmatrix} \begin{pmatrix} S_{00} & S_{01} & S_{02} \\ S_{10} & S_{11} & S_{12} \\ S_{20} & S_{21} & S_{22} \end{pmatrix} \begin{pmatrix} 1 & 0 & 0 & 0 & 0 \\ 0 & 1 & 0 & 0 & 0 \\ 0 & 0 & N_{m0} & N_{m1} & N_{m2} \end{pmatrix} & \cdots \\ \vdots & & \vdots \end{bmatrix} \begin{bmatrix} \vdots \\ \begin{pmatrix} \dot{A}_0 \\ A_1 \\ A_{m0} \\ A_{m1} \\ A_{m2} \end{pmatrix} \\ \vdots \end{bmatrix} = \begin{bmatrix} \vdots \\ \begin{pmatrix} 1 & 0 & 0 \\ 0 & 1 & 0 \\ 0 & 0 & N_{m0} \\ 0 & 0 & N_{m1} \\ 0 & 0 & N_{m2} \end{pmatrix} \begin{pmatrix} P_0 \\ P_1 \\ P_2 \end{pmatrix} \\ \vdots \end{bmatrix}. \tag{16}$$

$$\begin{bmatrix} \vdots & & \vdots \\ \cdots & \begin{pmatrix} 1 & 0 & 0 \\ 0 & 1 & 0 \\ 0 & 0 & N_{m0} \\ 0 & 0 & N_{m1} \\ 0 & 0 & N_{m2} \end{pmatrix} \begin{pmatrix} S_{00} & S_{01} & S_{02}N_{m0} & S_{02}N_{m1} & S_{02}N_{m2} \\ S_{10} & S_{11} & S_{12}N_{m0} & S_{12}N_{m1} & S_{12}N_{m2} \\ S_{20} & S_{21} & S_{22}N_{m0} & S_{22}N_{m1} & S_{22}N_{m2} \end{pmatrix} & \cdots \\ \vdots & & \vdots \end{bmatrix} \begin{bmatrix} \vdots \\ \begin{pmatrix} \dot{A}_0 \\ A_1 \\ A_{m0} \\ A_{m1} \\ A_{m2} \end{pmatrix} \\ \vdots \end{bmatrix} = \begin{bmatrix} \vdots \\ \begin{pmatrix} \dot{P}_0 \\ P_1 \\ P_2N_{m0} \\ P_2N_{m1} \\ P_2N_{m2} \end{pmatrix} \\ \vdots \end{bmatrix}. \tag{17}$$

$$\begin{bmatrix} \vdots & & \vdots \\ \cdots & \begin{pmatrix} S_{00} & S_{01} & S_{02}N_{m0} & S_{02}N_{m1} & S_{02}N_{m2} \\ S_{10} & S_{11} & S_{12}N_{m0} & S_{12}N_{m1} & S_{12}N_{m2} \\ N_{m0}S_{20} & N_{m0}S_{21} & N_{m0}S_{22}N_{m0} & N_{m0}S_{22}N_{m1} & N_{m0}S_{22}N_{m2} \\ N_{m1}S_{20} & N_{m1}S_{21} & N_{m1}S_{22}N_{m0} & N_{m1}S_{22}N_{m1} & N_{m1}S_{22}N_{m2} \\ N_{m2}S_{20} & N_{m2}S_{21} & N_{m2}S_{22}N_{m0} & N_{m2}S_{22}N_{m1} & N_{m2}S_{22}N_{m2} \end{pmatrix} & \cdots \\ \vdots & & \vdots \end{bmatrix} \begin{bmatrix} \vdots \\ \begin{pmatrix} \dot{A}_0 \\ A_1 \\ A_{m0} \\ A_{m1} \\ A_{m2} \end{pmatrix} \\ \vdots \end{bmatrix} = \begin{bmatrix} \vdots \\ \begin{pmatrix} \dot{P}_0 \\ P_1 \\ P_2N_{m0} \\ P_2N_{m1} \\ P_2N_{m2} \end{pmatrix} \\ \vdots \end{bmatrix}. \tag{18}$$

The magnetic field equation (1) is simplified as

$$lp\nabla\cdot(\nu\nabla A) = -lp\nu\mu_0\left(\frac{\partial M_y}{\partial x} - \frac{\partial M_x}{\partial y}\right) - \frac{ld_pN}{Sa}i_w. \tag{19}$$

To simplify programming and avoid relocation of computer memory, the structure of the sparse coefficient matrix is kept largely the same as that of (5). Only $-\boldsymbol{C}_{12}$ and $-\boldsymbol{C}_{ll}$ are replaced by a unit matrix $\boldsymbol{I}$; $\boldsymbol{C}_{12}, \boldsymbol{C}_{1l}, \boldsymbol{D}_{11}, \boldsymbol{D}_{21}, \boldsymbol{D}_{l1}$ and $\boldsymbol{P}_l$ are set to be zero; the right-hand side of the first row in (5) is extended to include the current excitations. Equation (5) becomes

$$\begin{bmatrix} \boldsymbol{C}_{11} & 0 & 0 \\ 0 & \boldsymbol{I} & 0 \\ 0 & 0 & \boldsymbol{I} \end{bmatrix} \begin{Bmatrix} \boldsymbol{A} \\ \boldsymbol{i}_{\mathrm{ad}} \\ \boldsymbol{i}_l \end{Bmatrix} = \begin{Bmatrix} \boldsymbol{P} + \boldsymbol{C}_{13}\boldsymbol{i}_w \\ 0 \\ 0 \end{Bmatrix}. \tag{20}$$

After the first step, the eddy current and the electric circuit are taken into account. The normal matrix equation (5) is solved.

B. Having Mechanical Motion

If there is mechanical motion and its initial speed is not equal to zero, changes in the magnetic field due to the moving objects will induce eddy current in the solid conductors and back EMF in the windings. In such case the derivative $\partial\boldsymbol{A}/\partial t$ at $t = 0$ must be estimated. The proposed procedures are:

1) The time stepping starts from $t = -2\Delta t, -\Delta t, 0, \ldots$ (where Δt is the time step size). At $t = -2\Delta t$, only the magnetostatic field is solved. All conductivities are set to zero. After the first step, that is, from $t = -\Delta t$, the eddy-current will be accounted for and the conductivities are set to their normal values.
2) Speed is kept at its initial constant speed when $t \le 0$. The mechanical coupling algorithm is disabled.
3) The currents of all windings are kept at their initial values of $i = i(0)$ when $t \le 0$.

The solutions at $t = -2\Delta t$ and $t = -\Delta t$ are only used to estimate the derivatives at $t = 0$. The results when $t < 0$ are not output to users.

IV. Implementation of Adaptive Time Step Size

A. Relative Local Truncation Error

The implicit backward Euler's method is used to discretize the time variable. Using Taylor's expansion at the kth step, the local truncation error is [10]

$$e^* = x^k - x^k_* = -\frac{(\Delta t)^2}{2}x''(\xi^*). \tag{21}$$

If the forward Euler's method (explicit method) is used, and its solution is $x^{\#}$, the local truncation error is

$$e^{\#} = x^k - x^k_{\#} = \frac{(\Delta t)^2}{2}x''(\xi^{\#}). \tag{22}$$

Subtracting (21) from (22), and using differential mean-value theorem, one has

$$\begin{aligned} x^k_* - x^k_{\#} &= \frac{(\Delta t)^2}{2}x''(\xi^{\#}) + \frac{(\Delta t)^2}{2}x''(\xi^*) \\ &= (\Delta t)^2 x''(\xi), \\ \xi &\in [\xi^{\#}, \xi^*] \text{ or } \xi \in [\xi^*, \xi^{\#}]. \end{aligned} \tag{23}$$

Assuming $x''(\xi^*) = x''(\xi)$, and substituting (23) into (21), the local truncation error of the backward Euler's method is

$$e^* = \frac{1}{2}(x^k_{\#} - x^k_*) \tag{24}$$

where x^k_* is the solution of the backward Euler's method at the kth step; $x^k_{\#}$ is the solution of the forward Euler's method at the kth step.

The solution of the forward Euler's method $x^k_{\#}$ can be directly obtained from the previous solutions. The system equation (5) can be simply written as

$$Dx + B\frac{\partial x}{\partial t} = P. \tag{25}$$

Using the backward Euler's method at the $(k-1)$th step, one has

$$D^{k-1}x^{k-1} + B^{k-1}\frac{x^{k-1} - x^{k-2}}{(\Delta t)^{k-1}} = P^{k-1}. \tag{26}$$

Using the forward Euler's method at the kth step, one has

$$D^{k-1}x^{k-1} + B^{k-1}\frac{x^k_{\#} - x^{k-1}}{(\Delta t)^k} = P^{k-1}. \tag{27}$$

Comparing (26) and (27), one has the error indicator of the local truncation error

$$e^k_x = \frac{1}{2}\left[x^{k-1} + (x^{k-1} - x^{k-2})\frac{(\Delta t)^k}{(\Delta t)^{k-1}} - x^k\right]. \tag{28}$$

It can be interpreted as either the changing rate of the solutions or as the difference between the predicted solution and the true solution.

In the 2-D transient FEM solver, the unknown variables are

$$\boldsymbol{x} = \begin{Bmatrix} \boldsymbol{A} \\ \boldsymbol{i}_{\mathrm{ad}} \\ \boldsymbol{i}_l \end{Bmatrix}. \tag{29}$$

If the absolute values of the local truncation errors of different variables are used, and because $\boldsymbol{A}, \boldsymbol{i}_{\mathrm{ad}}$ and $\boldsymbol{i}_l$ have different dimensions, errors from those variables having small values will be ignored; if the relative value e_x/x of the local truncation error is used, when x is equal to zero, the error will become infinite. In this paper a mixed absolute-relative "norm" is proposed to form a scalar error estimation that properly includes the effects from all variables:

$$e_x = \sqrt{\sum_i \left(\frac{\|e^k_i\|}{\max(\|x_i\|, S_i)}\right)^2} \tag{30}$$

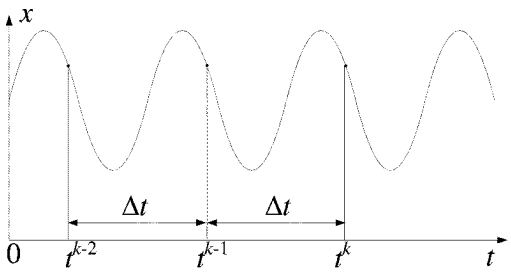

Fig. 2. A periodic function.

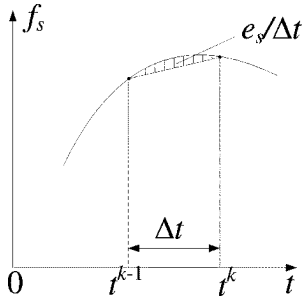

Fig. 3. Discretization error of a source.

where $||x_i|| = \sqrt{\sum_i x_i^2}$. To prevent zero or very small value of $||x_i||$ so that e_x/x will not become infinite, a prescribed temporal tolerance value S_i for different physical quantities is introduced in (30).

B. Consideration of Motion

In the transient solvers, the mechanical force/torque balance equation is coupled indirectly; the position at the kth step is predicted from the last step. Therefore, its accuracy can be ensured only if the speed of the adjacent steps does not change drastically. To consider this issue, the speed s is also included in the error controller. The variable column matrix $\boldsymbol{x}$ becomes

$$\boldsymbol{x} = \begin{Bmatrix} \boldsymbol{A} \\ \boldsymbol{i}_{\rm ad} \\ \boldsymbol{i}_l \\ s \end{Bmatrix}. \tag{31}$$

Good control of the step size ensures high solution accuracy for the indirect coupling of the mechanical balance equation.

C. Discretization Error of Excitations

If only the local truncation error is used to control the step size, it has some limitations as described below.

1) If the step size is too large, the estimated error may be incorrect. Here is a typical example when considering an extreme situation: if x is a periodic function with the period T, and if $\Delta t = T$, the estimated error of x becomes zero (see Fig. 2). Such conclusion is obviously incorrect.
2) If there are no $\partial x/\partial t$ terms, the local truncation error should be equal to zero.

Therefore, the discretization error of the sources should also be accounted for. If the source is a function f_s, as shown in Fig. 3, its error indicator is

$$e_s^k = \frac{1}{(\Delta t)} \left| \int_{t^{k-1}}^{t^k} |f_s(t)| dt - \frac{|f_s(t^{k-1})| + |f_s(t^k)|}{2} (\Delta t) \right|. \tag{32}$$

According to trapezoidal rule, one has

$$e_s^k = \frac{1}{(\Delta t)} \left| \frac{f''_s(\xi)}{12} (\Delta t)^3 \right| = \left| \frac{f''_s(\xi)}{12} (\Delta t)^2 \right| \propto (\Delta t)^2. \tag{33}$$

A relative "norm" is used to form the scalar error estimate

$$e_s = \sqrt{\sum_i \left(\frac{||e_s^k||}{\max(||f_s||, S_i)} \right)^2}. \tag{34}$$

D. The Total Time Stepping Error

Usually, if the step size is small enough, $e_s < e_x$; if the step size is too large, it is likely that $e_s > e_x$. The total time stepping error is the geometric average of e_x and e_s:

$$e = \sqrt{e_x^2 + e_s^2}. \tag{35}$$

E. Basic Formulation for Adjusting the Step Size

Because e^k is approximately proportional to $(\Delta t)^p$ (for backward Euler's method $p = 2$), the predicted step size for the next step is

$$(\Delta t)^{k+1} = K_{\rm SF} (\Delta t)^k \left(\frac{e_{\rm tolerance}}{e^k} \right)^{\frac{1}{p}} \tag{36}$$

where $e_{\rm tolerance}$ is the tolerance of the error; e^k is the error at the kth step. The coefficient $K_{\rm SF} = 0.75$ is a safety factor to ensure the error size is neither too large nor too small.

At the step $k+1$, if $e^{k+1} > e_{\rm tolerance}$, this step size will be rejected. The updated step size is

$$(\Delta t)^{k+1} = K_{\rm SF} (\Delta t)^{k+1}_{\rm last\_computation} \left(\frac{e_{\rm tolerance}}{e^{k+1}_{\rm last\_computation}} \right)^{\frac{1}{p}} \tag{37}$$

where $(\Delta t)^{k+1}_{\rm last\_computation}$ and $e_{\rm last\_computation}$ are the step size (rejected) and the error at the step $k+1$, respectively. Because the computed error is from the same step, the value of $K_{\rm SF}$ can be slightly larger; here $K_{\rm SF} = 0.9$.

After successive rejections, the approximate exponent can be obtained from

$$p = \frac{\log(\Delta t)_n - \log(\Delta t)_{n-1}}{\log e_n - \log e_{n-1}}. \tag{38}$$

F. Prevention of the Changing of the Step Size Too Large

The limitation to guard against changes in the step size becoming too large should be applied because:

1) If the step size changes too quickly, the predicted error may be incorrect occasionally, i.e., $|e^k - e^{k+1}|$ could be too large and rejection at the next step may need to be invoked.
2) In the solver if there are 2nd order derivative terms such as

$$\frac{{\rm d}^2 x^k}{{\rm d}t^2} = \frac{\left(\frac{x^k - x^{k-1}}{(\Delta t)^k} \right) - \left(\frac{x^{k-1} - x^{k-2}}{(\Delta t)^{k-1}} \right)}{(\Delta t)^k} + \frac{e^k - e^{k-1}}{(\Delta t)^k} \tag{39}$$

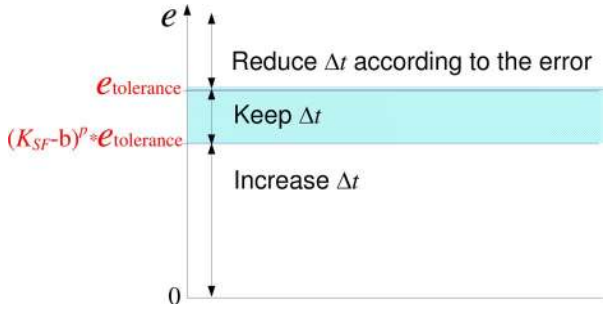

Fig. 4. The control strategy of adaptive step size.

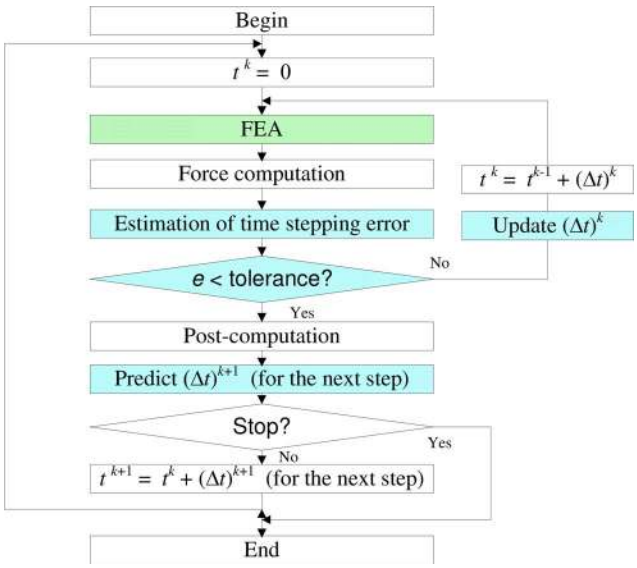

Fig. 5. Block diagram of the adaptive time stepping algorithm.

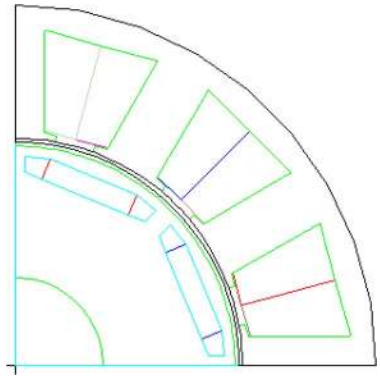

Fig. 6. A PM motor.

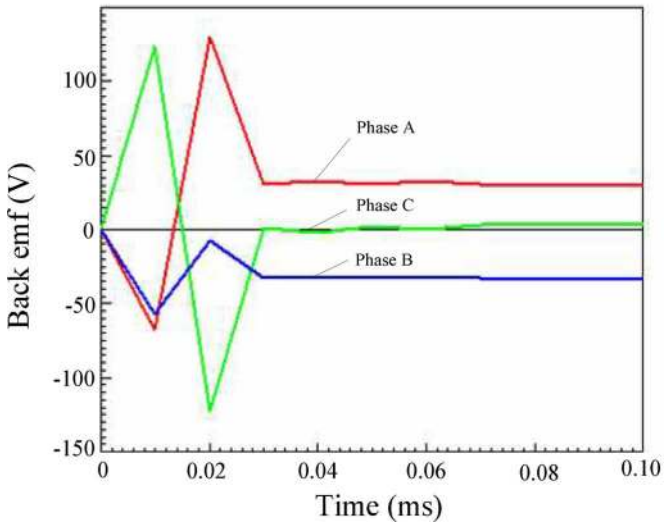

Fig. 7. Computed back EMF using normal method.

the error of the 2nd order derivative terms $(e^k - e^{k-1})/((\Delta t)^k)$ will be large [9].

Therefore, the following protection measures are included in the program:

1) If the error is smaller than $e_{\text{tolerance}}$ but larger than $(K_{\text{SF}} - b)^p e_{\text{tolerance}}$ (where $b = 0.1$), the step size will be kept the same (Fig. 4).
2) When rejection occurs, each pair of $(\Delta t, e)$ is stored. If further reduction of step size cannot reduce the error, the step size that has the smallest error will be used.
3) When the magnetic field is coupled with the external circuits and if there are switching elements, the external circuits will govern the maximum step size allowed. That is, during the time t to $t + \Delta t$, it is supposed that the statuses of all switching elements are kept unchanged. Therefore, in the FEM solver, if $\Delta t \geq (\Delta t)_{\max\_\text{external\_circuits}}$, set $\Delta t = (\Delta t)_{\max\_\text{external\_circuits}}$, where $(\Delta t)_{\max\_\text{external\_circuits}}$ is the maximum step size allowed from the external circuit.
4) To provide flexibility to users, the users can specify the minimum step size $(\Delta t)_{\min}$ and maximum step size $(\Delta t)_{\max}$, and in the program $(\Delta t)_{\min} \leq \Delta t \leq (\Delta t)_{\max}$.

The block diagram of the adaptive time stepping algorithm is shown in Fig. 5. At each time step, after the computation of the magnetic field, the time stepping error will be estimated. If the error is larger than the tolerance, the step size will be modified and the field of this step will be solved again; if the error is less than the tolerance, the step size for the next time step will be predicted and the algorithm will go to the next time step.

V. Application Examples

A. Steady-State Operation of a Y-Connected PM Motor

The first example is to simulate the steady-state operation of a Y-connected PM motor running at 3485 rpm (Fig. 6). Comparison of the computed results of back EMF, current, and torque obtained using the normal method and the proposed method, respectively, are shown in Figs. 7–12. One notes that nonphysical solutions at the starting of the simulation have been successfully eliminated. Fig. 7 shows the computed back EMF using the normal method and it can be seen that the back EMF curves have big spikes at $t = \Delta t$ and $t = 2\,\Delta t$. Fig. 10 shows the computed back EMF using the proposed method in which the back EMF curves are very smooth at $t = \Delta t$ and $t = 2\Delta t$.

B. An Induction Motor Driven by a Pulsewidth Voltage

The second example is an induction motor (Fig. 13) driven by a pulsewidth voltage inverter. The waveform of the pulsewidth voltage is shown in Fig. 14. The time step size when using automatic adaptive step size algorithm is shown in Fig. 15. The

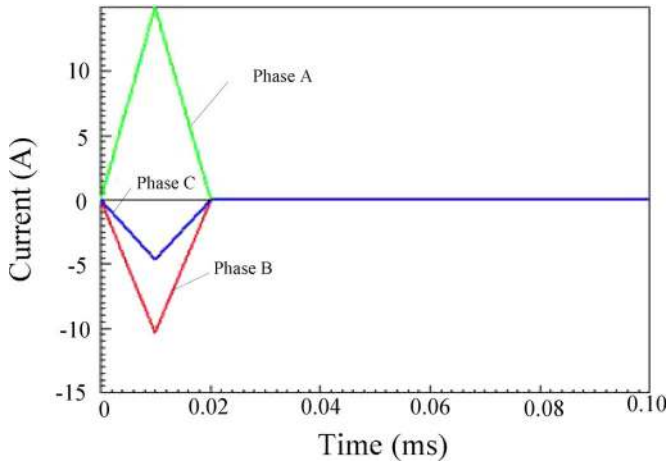

Fig. 8. Computed current using normal method.

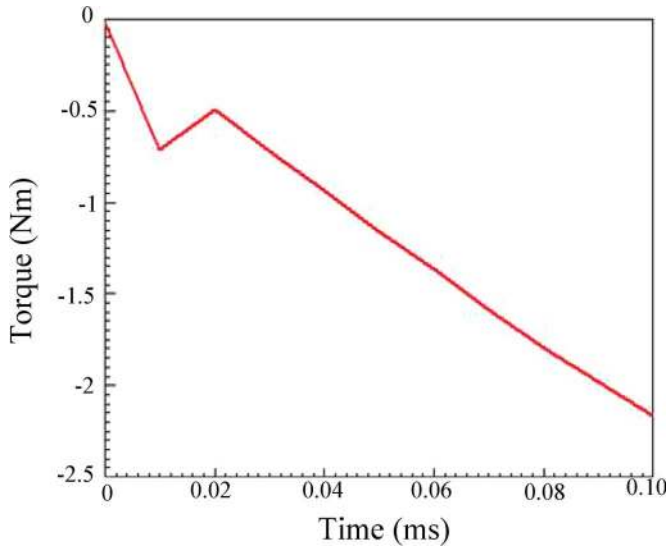

Fig. 9. Computed torque using normal method.

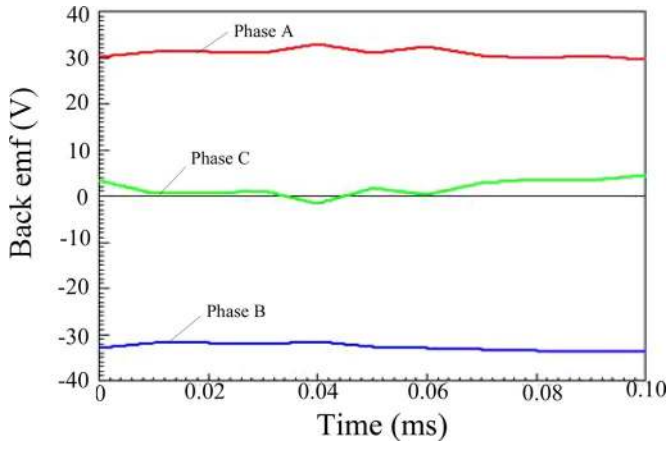

Fig. 10. Computed back EMF using proposed method.

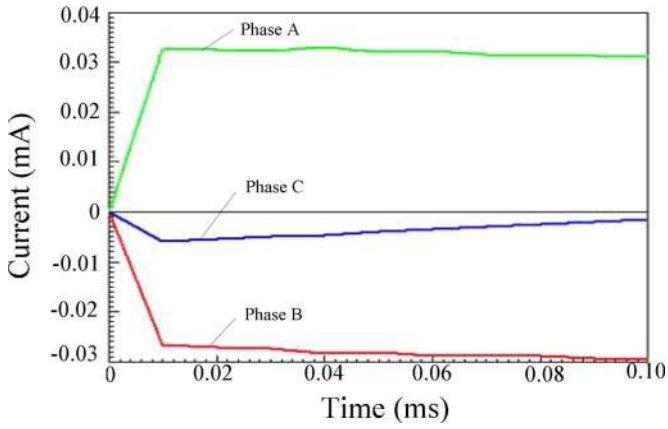

Fig. 11. Computed current using proposed method.

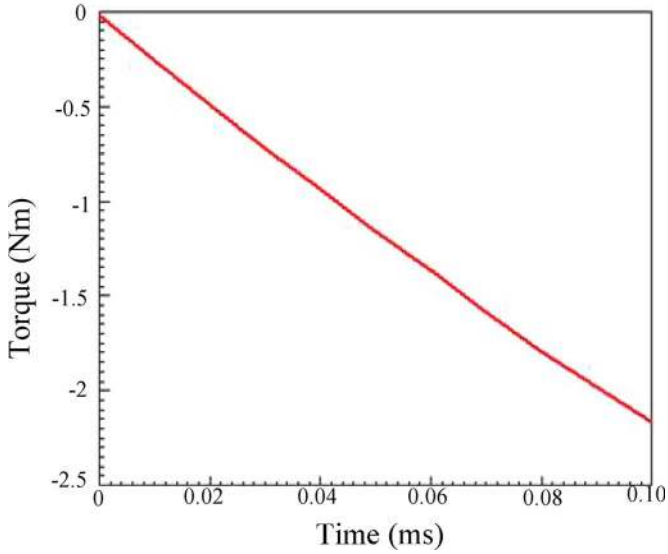

Fig. 12. Computed torque using proposed method.

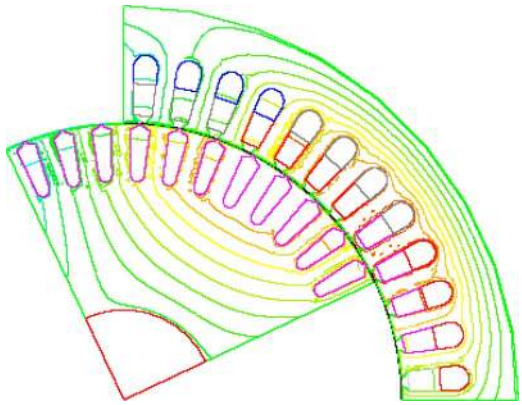

Fig. 13. An induction motor.

time stepping error when using fixed step size 11×10^{-5} s is shown in Fig. 16. The time stepping error when using adaptive step size algorithm is shown in Fig. 17.

If using a fixed step size $\Delta t = 1 \times 10^{-}5$ s, the time stepping number is 300. With the use of the proposed adaptive time step size and if the error tolerance is 10^{-5}, the time stepping number is 131. For this example, the computing time is reduced by about 56%.

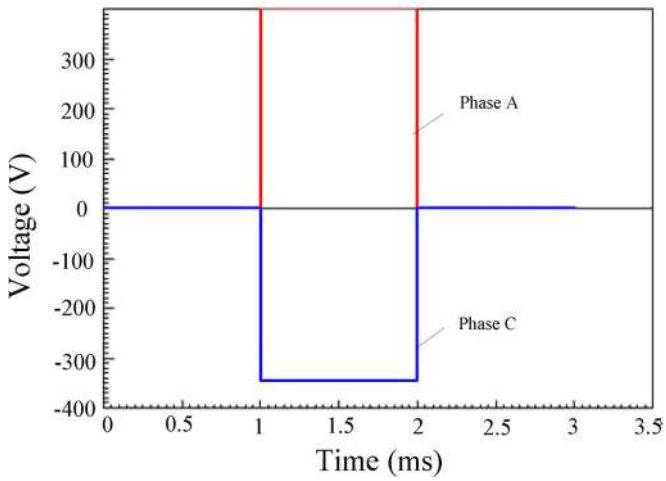

Fig. 14. The input PWM voltage of the induction motor.

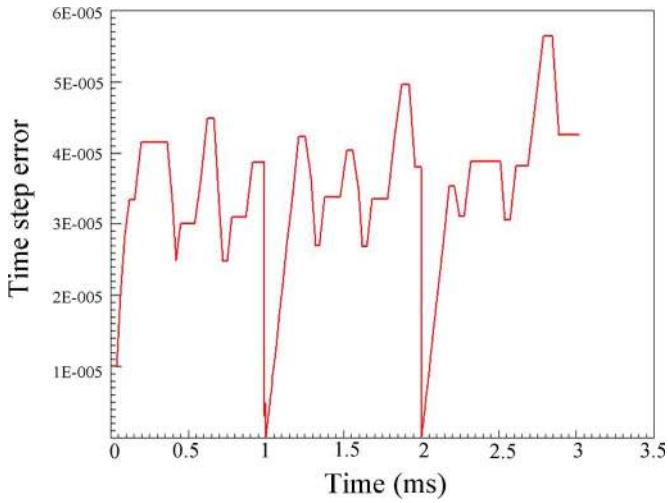

Fig. 15. The time step size when using automatic adaptive step size algorithm.

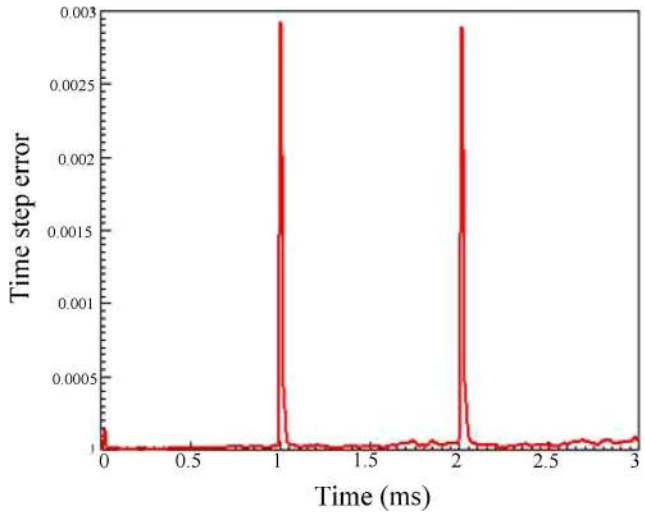

Fig. 16. The time stepping error when using fixed step size.

C. A Transient Model of Windings for Steep-Front Surges

The third example is a transient model of windings (Fig. 18) for steep-front surges. A step voltage (simulating the PWM wavefront) having a 50 ns rise-time and 800 V magnitude is applied to the terminals of the cable. The coil is modeled as solid conductors to include eddy-current effect (Fig. 19). The feeding cable is represented by an external circuit (Fig. 20). If a fixed step size ($\Delta t = 8 \times 10^{-10}$ s) is used, the time stepping number is 20000 and the CPU time is 93 h. If adaptive step size algorithm is used, the time stepping number is 442 and the CPU time is only 125 min, which means the computing time is dramatically reduced. The step size and the time stepping error are shown in Figs. 21 and 22, respectively. The computed node voltage distribution including the effect from the feeder cable

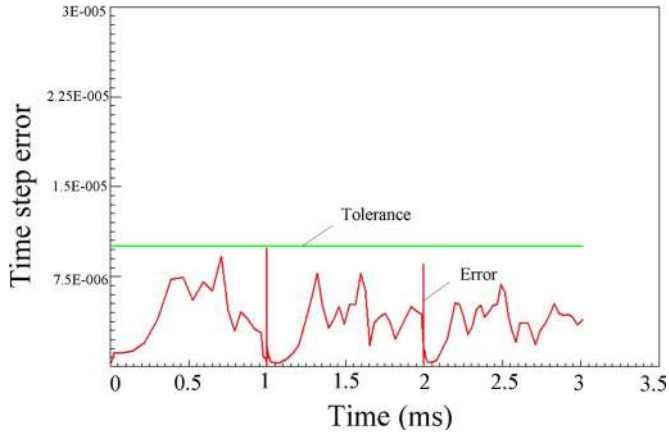

Fig. 17. The time stepping error when using adaptive step size algorithm.

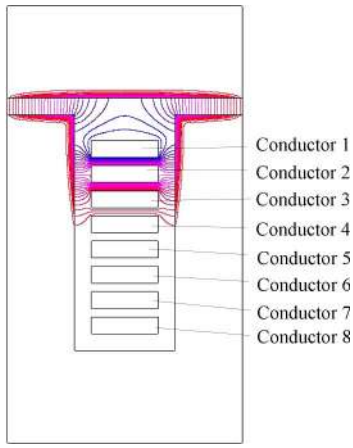

Fig. 18. Slot section of a form-wound coil and its flux plot when $t = 10^{-8}$ s.

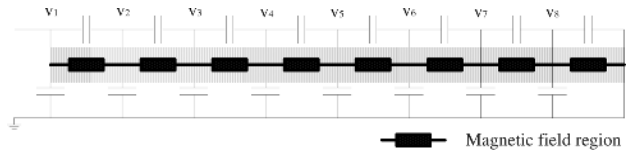

Fig. 19. Coil circuit for voltage distribution analysis.

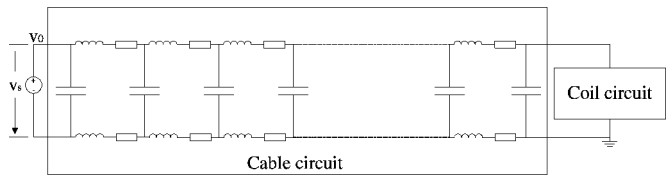

Fig. 20. The coil is connected to a step voltage through a long cable.

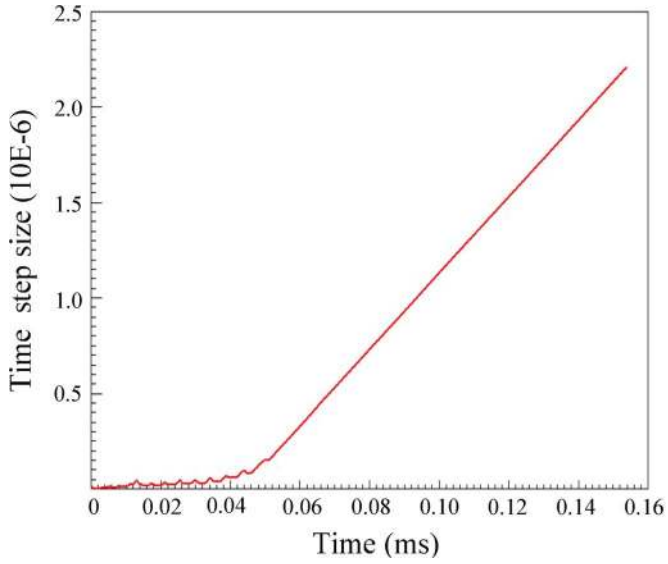

Fig. 21. Automatic adaptive time step size. (Step size changes from 8×10^{-10} s to 2×10^{-6} s.)

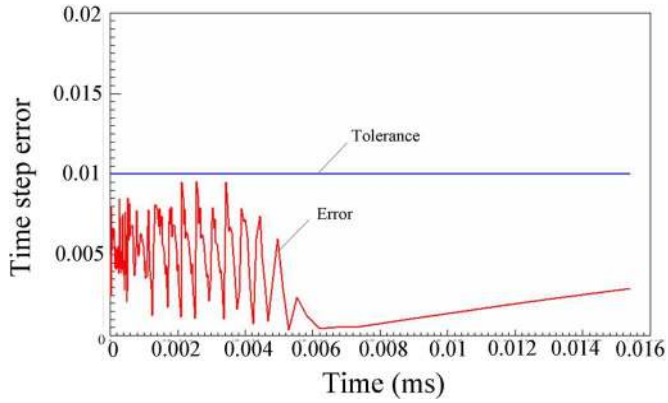

Fig. 22. Time stepping error when using adaptive time step size algorithm.

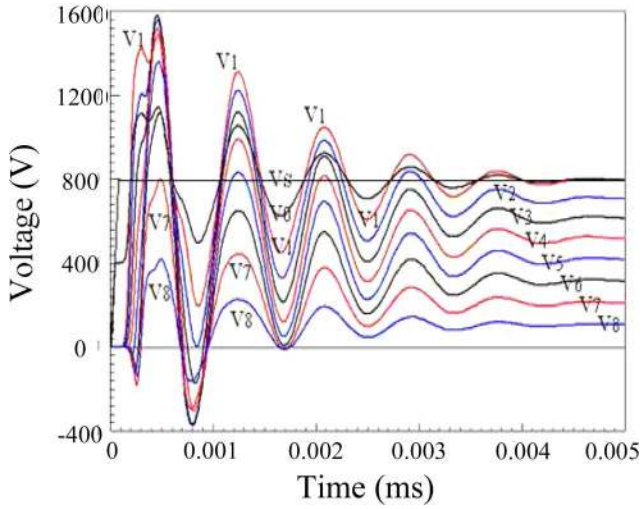

Fig. 23. Node voltage distribution including the effect from the feeder cable.

is shown in Fig. 23. A typical distribution of current density in the conductors when $t = 8 \times 10^{-7}$ s is shown in Fig. 24. The computed back EMF is shown in Fig. 25.

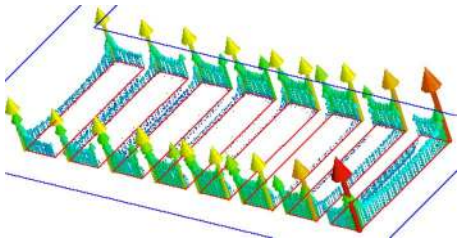

Fig. 24. Distribution of current density in the conductors when$t = 8 \times 10^{-7}$ s.

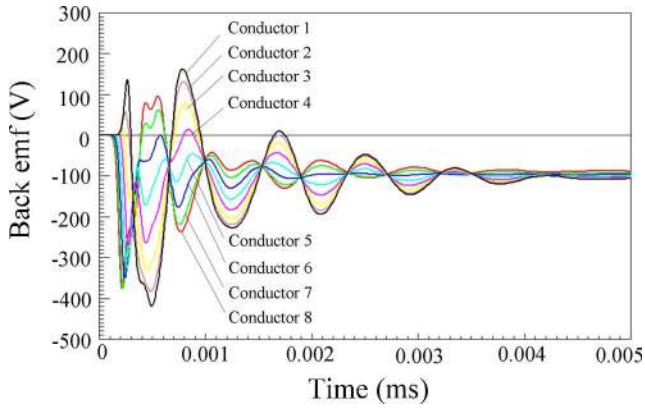

Fig. 25. Computed back EMF in conductors.

VI. Conclusion

At the first step of time-stepping FEM, the magnetostatic field is solved to obtain a reasonable initial field distribution. If there is mechanical motion and its initial speed is not equal to zero, the integrating time can start from a negative time $t = -2\Delta t$ in order to evaluate the derivatives at $t = 0$. For adaptive step size algorithm, a proper relative local truncation error is presented. When determining the step size, the discretization error of the excitations should be accounted for. The program should also prevent the step size from changing too quickly. The proposed algorithm can automatically determine the time step size at each time step. It reduces computing time while controlling the time stepping error to within specified tolerances. Almost no additional computation time is required. It is robust to a wealth of problems.

Acknowledgment

This work was supported in part by The Hong Kong Polytechnic University under Grants U489 and 87RX.

References

[1] J. Faiz, B. M. Ebrahimi, B. Akin, and H. A. Toliyat, "Comprehensive eccentricity fault diagnosis in induction motors using finite element method," *IEEE Trans. Magn.*, vol. 45, no. 3, pp. 1764–1767, Mar. 2009.

[2] Z. Gmyrek, A. Boglietti, and A. Cavagnino, "Estimation of iron losses in induction motors: Calculation method, results and analysis," *IEEE Trans. Ind. Electron.*, accepted for publication.

[3] L. Jian, K. T. Chau, and J. Z. Jiang, "A magnetic-geared outer-rotor permanent-magnet brushless machine for wind power generation," *IEEE Trans. Ind. Appl.*, vol. 45, no. 3, pp. 954–962, May–Jun. 2009.

[4] W. N. Fu, S. L. Ho, and Z. Zhang, "Design of position detection strategy of sensorless permanent magnet motors at standstill using transient finite element analysis," *IEEE Trans. Magn.*, vol. 45, no. 10, pp. 4668–4671, Oct. 2009.

[5] S. L. Ho, J. Wang, W. N. Fu, and Y. H. Wang, "A novel crossed traveling wave induction heating system and finite element analysis of eddy current and temperature distributions," *IEEE Trans. Magn.*, vol. 45, no. 10, pp. 4777–4780, Oct. 2009.
[6] Y. B. Li, S. L. Ho, W. N. Fu, and W. Y. Liu, "Analysis and solution on squeak noise of small permanent magnetic DC brush motors in variable speed applications," *IEEE Trans. Magn.*, vol. 45, no. 10, pp. 4752–4755, Oct. 2009.
[7] Y. B. Li, S. L. Ho, W. N. Fu, and W. Y. Liu, "An interpolative finite-element modeling and the starting process simulation of a large solid pole synchronous machine," *IEEE Trans. Magn.*, vol. 45, no. 10, pp. 4605–4608, Oct. 2009.
[8] W. N. Fu, P. Zhou, D. Lin, S. Stanton, and Z. J. Cendes, "Modeling of solid conductors in two-dimensional transient finite-element analysis and its application to electric machines," *IEEE Trans. Magn.*, vol. 40, no. 2, pp. 426–434, Mar. 2004.
[9] W. N. Fu and S. L. Ho, "Enhanced nonlinear algorithm for the transient analysis of magnetic field and electric circuit coupled problems," *IEEE Trans. Magn.*, vol. 45, no. 2, pp. 701–706, Feb. 2009.
[10] S. L. Ho, W. N. Fu, and H. C. Wong, "Application of automatic choice of step size for time stepping finite element method to induction motors," *IEEE Trans. Magn.*, vol. 33, no. 2, pp. 1370–1373, Mar. 1997.
[11] W. N. Fu, Z. J. Liu, and C. Bi, "A dynamic model of the disk drive spindle motor and its applications," *IEEE Trans. Magn.*, vol. 38, no. 2, pp. 973–976, Mar. 2002.
[12] A. Arkkio, "Analysis of induction motors based on the numerical solution of the magnetic field and circuit equations," Helsinki, Acta Polytechnica Scandinavica, Electrical Engineering Series no. 59, 1987.
[13] W. N. Fu, S. L. Ho, H. L. Li, and H. C. Wong, "An improved nodal method for circuit and multi-slice magnetic field coupled finite element analysis," *Electr. Power Comp. Syst.*, vol. 32, no. 7, pp. 671–689, Jul. 2004.
[14] W. N. Fu, S. L. Ho, H. L. Li, and H. C. Wong, "A multislice coupled finite-element method with uneven slice length division for the simulation study of electric machines," *IEEE Trans. Magn.*, vol. 39, no. 3, pp. 1566–1569, May 2003.
[15] S. L. Ho and W. N. Fu, "A comprehensive approach to the solution of direct-coupled multi-slice model of skewed induction motors using time stepping eddy-current finite element method," *IEEE Trans. Magn.*, vol. 33, no. 3, pp. 2265–2273, May 1997.
[16] S. L. Ho, H. L. Li, and W. N. Fu, "Inclusion of inter-bar currents in a network-field coupled time stepping finite element model of skewed rotor induction motors," *IEEE Trans. Magn.*, vol. 35, no. 5, pp. 4218–4225, Sep. 1999.
[17] S. L. Ho, W. N. Fu, and H. C. Wong, "Direct modeling of the starting process of skewed rotor induction motors using a multi-slice technique," *IEEE Trans. Energy Convers.*, vol. 14, no. 4, pp. 1253–1258, Dec. 1999.

Weinong Fu received the Ph.D. degree in electrical engineering from The Hong Kong Polytechnic University, Hong Kong, in 1999.

Since October 2007, he has been an Associate Professor with The Hong Kong Polytechnic University. Previously, he was one of the key developers at Ansoft Corporation in the USA. During his seven years at Ansoft, he focused on the development of the commercial software Maxwell. He has published over 110 papers in journals and in leading conferences. His current research interests mainly focus on numerical methods of electromagnetic field computation, optimal design based on numerical models, applied electromagnetics, and novel electric motors.

Siu-Lau Ho received the B.Sc. and Ph.D. degrees in electrical engineering from the University of Warwick, Warwick, U.K.

He joined Hong Kong Polytechnic, Hong Kong, in 1979 and is now a Chair Professor in electricity utilization and the Head of Department of Electrical Engineering, The Hong Kong Polytechnic University. Since joining the university, he has actively worked with local industry, particularly in railway engineering. He is the holder of several patents and has published a wealth of publications, including over 200 conference papers and more than 140 papers in leading journals, mostly in the IEEE Transactions and IEE Proceedings. His main research interests include traction engineering, the application of finite elements in electrical machines, phantom loading of machines, and optimization of electromagnetic devices.